Magnet Temperature Detection of PMSM with Wireless Power Transfer

Ryo Hamba, Keisuke Kusaka
Dept. of Electrical, Electronics and Information Engineering
Nagaoka University of Technology
Niigata, Japan
s223138@stn.nagaokaut.ac.jp, kusaka@vos.nagaokaut.ac.jp

Yoshihisa Hojo
Development Center
Toyo Denki Seizo K.K.
Kanagawa, Japan
hohjoh@toyodenki.co.jp

***Abstract*—Temperature information of the magnet on permanent magnet synchronous motors (PMSMs) is crucial to prevent failures caused by the thermal demagnetization of magnets. This paper proposes a detection method for the magnet temperature of PMSMs using a wireless power transfer (WPT) system with a thermistor. The magnet temperature is measured by the NTC thermistor, which is connected to the secondary side of a WPT system. The temperature change of the magnet is detected through the change in the input power on the primary side. The prototype of the WPT system is designed and demonstrated based on the characteristics of the thermistor.**

Keywords—PMSM; temperature detection; wireless power transfer

I. INTRODUCTTION

With the spread of environmentally friendly electric and hybrid vehicles [1], the demand for permanent magnet synchronous motors (PMSMs) as their drive-power source is increasing. The PMSM tends to be more efficient than induction motors [2] since PMSMs do not require a secondary current. In contrast, magnets on a rotor in PMSMs generate heat due to eddy current losses [3]. Demagnetization due to heat generation from magnets reduces the performance of PMSMs [4] and eventually causes failure. So, accurate detection of the magnet temperature of PMSMs is one of the crucial technological needs. However, it is difficult to directly measure the magnet temperature because the magnets are embedded in or attached to a rotor. Thus, a temperature measurement technology for rotating bodies such as a rotor of PMSMs is required.

Slip rings, which have been used to transmit signals from a stationary body to a rotating body, have poor durability and maintenance problems because of contact between the brushes and the ring. A telemeter system using wireless communication has been proposed to solve the problem of slip rings [5]. Many components, such as the A/D converter, the CPU, and the wireless communication IC, must be attached to this system's rotating body. This causes an increase in cost.

Reference [6] proposes a method for indirectly estimating the magnet temperature of a PMSM by injecting a high-frequency current and estimating the stator inductance. This method only estimates the average temperature of all magnets and cannot detect partial magnet temperatures. References [7] and [8] have proposed a method to estimate the magnet temperature by modeling the PMSM in a thermal circuit. However, this method requires an accurate thermal model for temperature estimation.

This paper proposes a detection method of magnet temperature in the PMSM with a thermistor connected to the wireless power transfer (WPT) with magnetic field coupling [9]. This method solves the maintenance problem because there is no contact between the stationary and rotating parts. In addition, an accurate thermal model is not required. A prototype of the detecting system is designed and experimentally demonstrated. The input power of the WPT system varies with the temperature of the thermistor connected as a load on the secondary side.

II. TEMPERATURE DETECTION SYSTEM FOR ROTATING PARTS

A. System Configuration

Fig. 1 shows the configuration of the proposed PMSM magnet temperature detection system. The system comprises the stationary part and the rotating part. The stationary part consists of the power detection part and the power supply circuit, which includes the DC power supply, the high-frequency power supply, and the primary coil. The rotating part consists of the thermistor and the power receiving circuit, which includes the secondary coil. The thermistor is attached to the magnet, which is the temperature-detection target, on the rotor.

The power detection part detects the DC power supplied from the DC power supply to the high-frequency power supply. The high-frequency power supply and the primary coil transmit power to the power receiving circuit, including the secondary coil by WPT. The thermistor consumes power received from the power receiving circuit.

Fig. 2 shows the sketch of the proposed system with a PMSM. The primary and the secondary coils are inserted around the shaft. The power supply circuit is independent of the PMSM drive circuit. The thermistor and the power receiving circuit, including the secondary coil, rotate with the rotor.

B. Equivalent Circuit

This section presents a description of the operational principle of the proposed system, with reference to the equivalent circuit of the WPT system. Fig. 3 shows the T-type

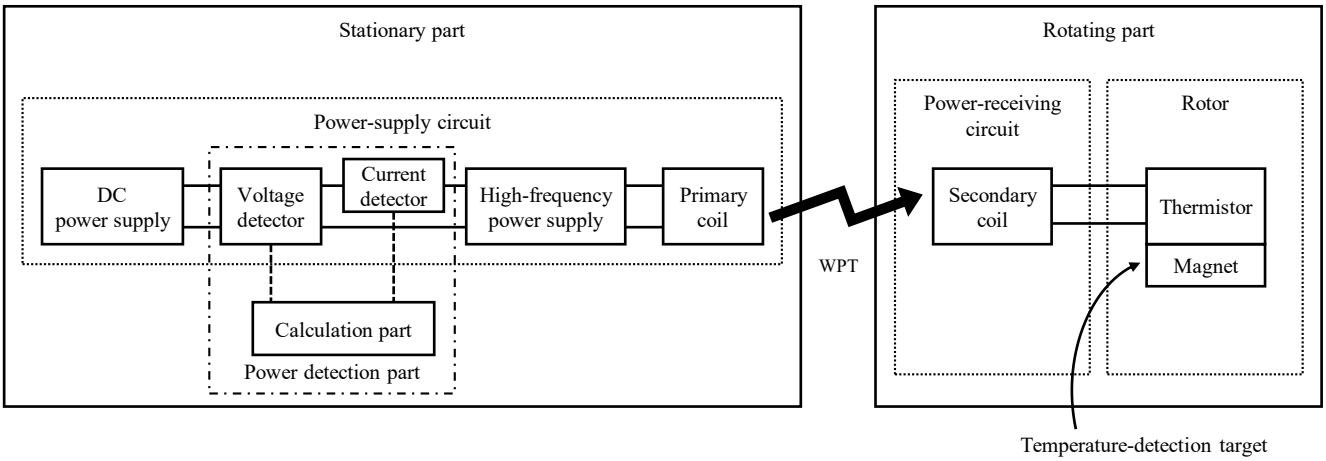

Fig. 1. PMSM magnet temperature detection system.

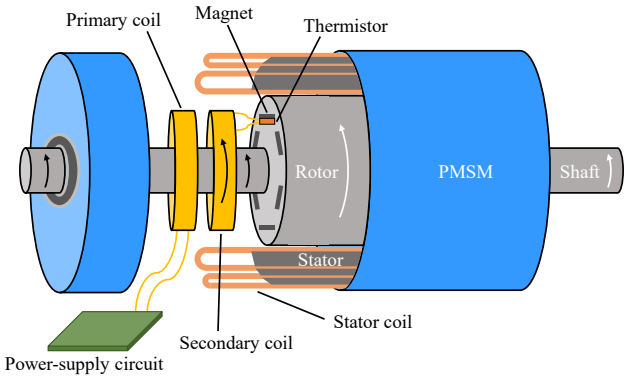

Fig. 2. Skech of the temperature detection system to a PMSM.

equivalent circuit of WPT for the temperature detection system. A series-series (S-S) compensation is used for the WPT system. The input current I_1 and the output current I_2 are shown in (1) and (2), respectively.

$$I_1 = \frac{r_2 + R_{th} + j\left(\omega L_2 - \frac{1}{\omega C_2}\right)}{\left\{r_1 + j\left(\omega L_1 - \frac{1}{\omega C_1}\right)\right\}\left\{r_2 + R_{th} + j\left(\omega L_2 - \frac{1}{\omega C_2}\right)\right\} + (\omega L_m)^2} V_1 \quad (1)$$

$$I_2 = \frac{j\omega L_m}{\left\{r_1 + j\left(\omega L_1 - \frac{1}{\omega C_1}\right)\right\}\left\{r_2 + R_{th} + j\left(\omega L_2 - \frac{1}{\omega C_2}\right)\right\} + (\omega L_m)^2} V_1 \quad (2)$$

When the resonance condition, as shown in (3), is satisfied, the input current I_1 and the output current I_2 are given by (4) and (5).

$$\omega_0 = \frac{1}{\sqrt{L_1 C_1}} = \frac{1}{\sqrt{L_2 C_2}} \quad (3)$$

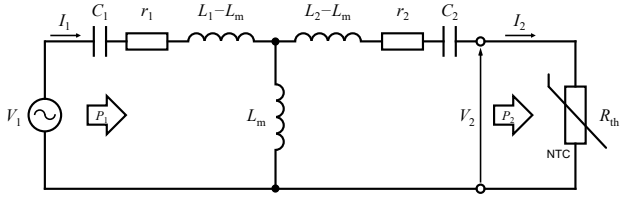

Fig. 3. T-type equivalent circuit of S-S conpensation topology WPT system for temperature detection system.

$$I_1 = \frac{r_2 + R_{th}}{r_1\left(r_2 + R_{th}\right) + \left(\omega L_m\right)^2} V_1 \quad (4)$$

$$I_2 = \frac{j\omega L_m}{r_1\left(r_2 + R_{th}\right) + \left(\omega L_m\right)^2} V_1 \quad (5)$$

Thus, the input power P_1 and the output power P_2 are given by (6) and (7). Equation (6) shows the dependence of the input power P_1 on the resistance of NTC thermistor R_{th}.

$$P_1 = \frac{r_2 + R_{th}}{r_1\left(r_2 + R_{th}\right) + \left(\omega L_m\right)^2} V_1^2 \quad (6)$$

$$P_2 = \frac{\left(\omega_0 L_m\right)^2}{\left\{r_1\left(r_2 + R_{th}\right) + \left(\omega_0 L_m\right)^2\right\}^2} V_1^2 R_{th} \quad (7)$$

The resistance of NTC thermistor R_{th} at absolute temperature T is shown in (8) using the B constant, where R_O is the resistance at the reference temperature T_O [10]. Equation (8) shows the dependence of the resistance of NTC thermistor R_{th} on the temperature T.

$$R_{th} = R_O \exp\left\{B\left(\frac{1}{T} - \frac{1}{T_O}\right)\right\} \tag{8}$$

Equations (6) and (8) mean that the input power P_1 depends on the temperature of the NTC thermistor T. Thus, the temperature change measured by the NTC thermistor connected to the secondary circuit appears as a change in the input power of the primary circuit.

III. Design and Simulation

A. Circuit design

The NTC thermistor used in the experiment has a power rating of 100 mW at an ambient temperature of 55°C [11]. Five of these thermistors are connected in parallel in the experiment therefore, the total power rating is 500 mW.

Table 1 shows the designed circuit parameters. The WPT circuit was designed in accordance with (9), which neglects the winding resistance r_1 and r_2 in (7), to ensure that the output power P_2 does not exceed the power rating of the NTC thermistor 500 mW when the load is the thermistor resistance R_{th} = 2 kΩ at room temperature 25°C. In the S-S compensation method, the output power decreases as the load decreases, so the output power will not exceed the rated power of the thermistor if the temperature exceeds 25°C. Resonant capacitors C_1 and C_2 are calculated by (3).

$$P_2 = \frac{V_1^2 R_{th}}{(\omega_0 L_m)^2} \tag{9}$$

B. Theoretical calculation and simulation

Fig. 4 shows the calculation and simulation result of input power P_1 and output power P_2 of the WPT system with respect to the temperature of the NTC thermistor T. The parameters shown in Table 1 are used for the calculation. V_1 is the R.M.S. value of the sine wave. In the calculation, the input power P_1 calculated by (6), the output power P_2 by (7), and the resistance of the NTC thermistor R_{th} by (8) are used where the B constant is 3977 K. In the simulation, the thermistor resistance is varied with changing the temperature, as shown in Fig. 5. Both calculated and simulated results show that the input power P_1 decreases monotonically with rising temperature T. So, the temperature of the NTC thermistor T can be detected from P_1. The results also show that the output power P_2 is less than the power rating of the NTC thermistor 500 mW at all temperatures.

TABLE I. Circuit Parameters

Parameter	Value
Primary side voltage V_1	0.5 V
Resonant frequency f	200 kHz
Primary side coil inductance L_1	80.9 μH
Secondary side coil inductance L_2	80.9 μH
Coupling coefficient k	0.30
Mutual inductance L_m	24.3 μH
Primary side coil resistance r_1	249 mΩ
Secondary side coil resistance r_2	249 mΩ
Primary side resonant capacitor C_1	7.83 nF
Secondary side resonant capacitor C_2	7.83 nF

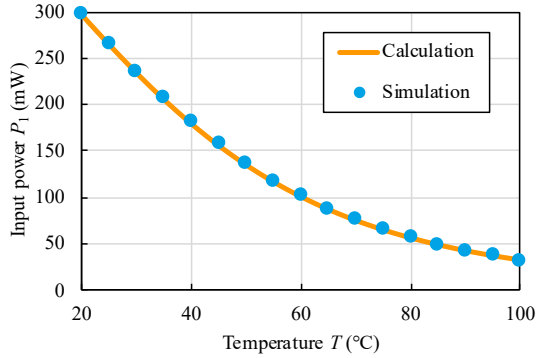

(a) Input power.

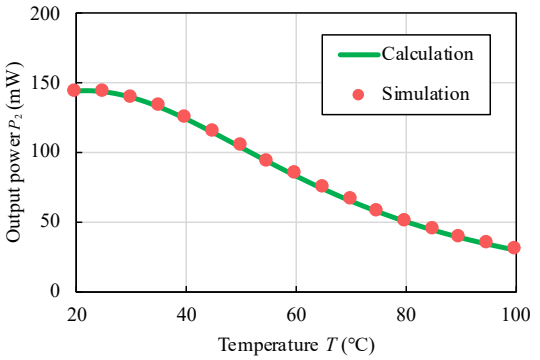

(b) Output power

Fig. 4. Calculation and simulation result of input power and output power vs. temperature of NTC thermistor.

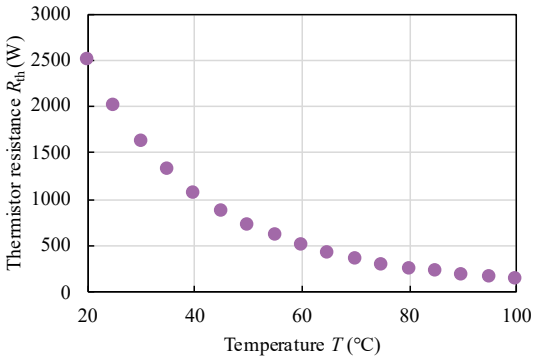

Fig. 5. Relationship between resistance of NTC thermistor and temperature.

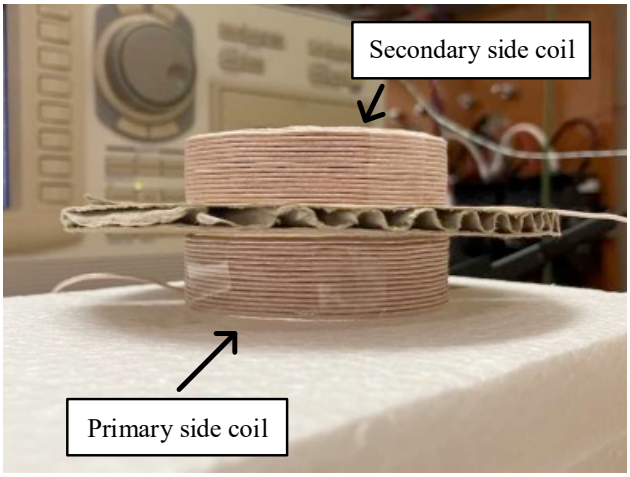

Fig. 6. Coils for experiment of WPT system.

TABLE II. COIL DIMENSIONS

Parameter	Value
Nagaoka coefficient K	0.379
Relative permeability μ_r	1.0
Diameter d	60 mm
Length l	16 mm
Turns N	31

TABLE III. COMPARISON OF THE DESIGNED AND MEASURED VALUES

Parameter	Designed value	Measured value
Primary side coil inductance L_1	80.9 μH	80.9 μH
Secondary side coil inductance L_2	80.9 μH	80.9 μH
Primary side coil resistance r_1	249 mΩ	430 mΩ
Secondary side coil resistance r_2	249 mΩ	480 mΩ
Matual inductance L_m	24.3 μH	25.4 μH
Coupling coefficient k	0.30	0.313
Primary side capacitor C_1	7.83 nF	7.83 nF
Secondary side capacitor C_2	7.83 nF	7.82 nF

IV. EXPERIMENTS

A. Prototype circuit

Fig. 6 shows the coils for the experimental setup. Air-core solenoid coils are used in the experiment. The coils are arranged so that the central axes are coincident. The air gap between the coils is 5 mm. The coil dimensions are shown in Table 2. Table 3 shows a comparison of the designed and measured values for the coils and resonant capacitors. The discrepancy between the design and measured values of the winding resistance can be attributed to the difference between the DC and AC resistances. The DC resistance is used for simplicity in the design.

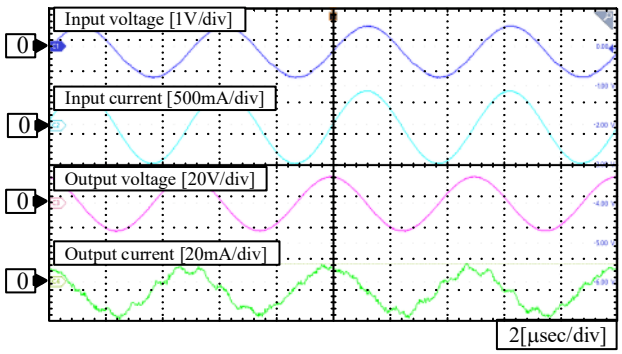

(a) At 30.8 °C.

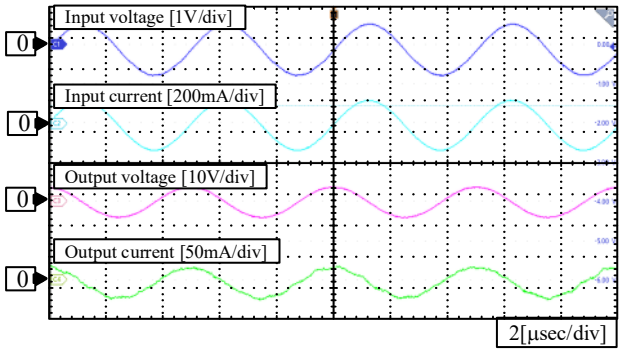

(b) At 83.9 °C.

Fig. 7. Waveforms of prototype WPT circuit.

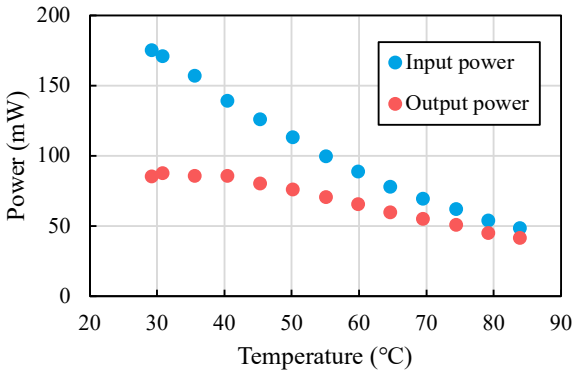

Fig. 8. Experimental result of input and output power vs. temperature of NTC thermistor.

Experiments were conducted based on the circuit shown in Fig. 3. The supply voltage V_1 is a sine wave. The NTC thermistor was placed and heated in a thermostatic chamber. A thermocouple measured the temperature of the NTC thermistor.

B. Experimental Results

Fig. 7 shows the input/output voltage and current waveforms of the prototype WPT system. Input voltage and current, and output voltage and current are in phase, respectively. In addition,

TABLE IV. CIRCUIT PARAMETERS FOR EXPERIMENT WITH SHAFT

Parameter	Value
Primary side voltage V_1	3.0 V
Resonant frequency f	224.4 kHz
Primary side coil inductance L_1	64.2 μH
Secondary side coil inductance L_2	68.6 μH
Coupling coefficient k	0.247
Mutual inductance L_m	16.4 μH
Primary side coil resistance r_1	7.83 Ω
Secondary side coil resistance r_2	7.82 Ω
Primary side resonant capacitor C_1	7.83 nF
Secondary side resonant capacitor C_2	7.83 nF

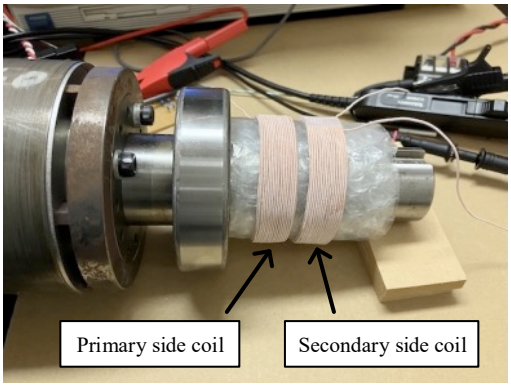

Fig. 9. Coils with inserted shaft of the rotor.

the output has a phase-lead of 90° with the input. Thus, this circuit operates resonantly even if the temperature changes.

Fig. 8 shows the change in the input and output power with respect to temperature change. The input power decreases monotonically with rising temperature. The same characteristics as in theoretical calculations and simulations are obtained. The output power is always below 500 mW, the power rating of the thermistor.

V. EFFECTS OF SHAFT

It is anticipated that the coils will be affixed around the shaft, as depicted in Fig. 2. As a steel shaft penetrates through the center of the coils, iron loss and other effects will not be ignored. In this section, the effect by the shaft is experimentally evaluated.

A. Experimental conditions

Table 4 shows the circuit parameters for the experiment with the shaft. The coils are the same as in the experiment in the previous section, but the inductances of the coils L_1 and L_2 and the AC resistances of the windings r_1 and r_2 have changed from the values shown in Table 3 because of the steel shaft. To prevent the thermistor power consumption from decreasing due to the increased winding resistance, the supply voltage V_1 was

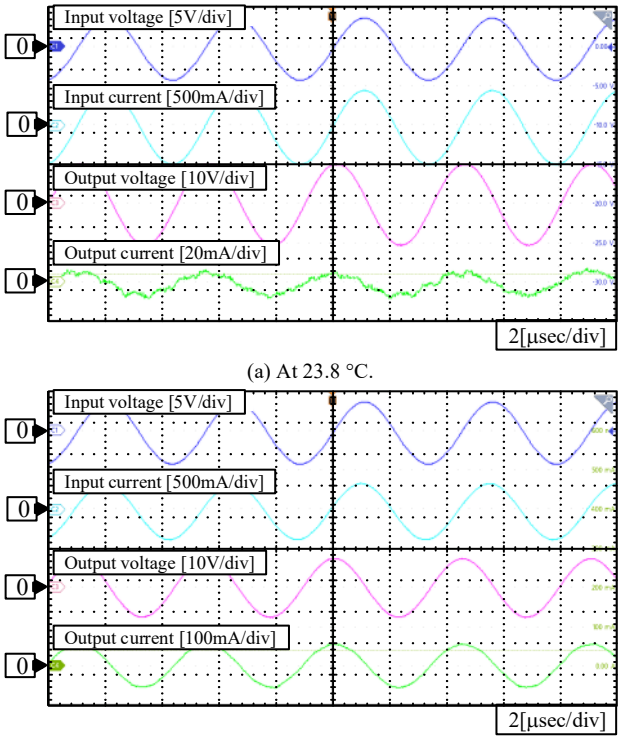

(a) At 23.8 °C.

(b) At 86.8 °C

Fig. 10. Waveforms of the WPT system when the coils are mounted on the shaft of the rotor.

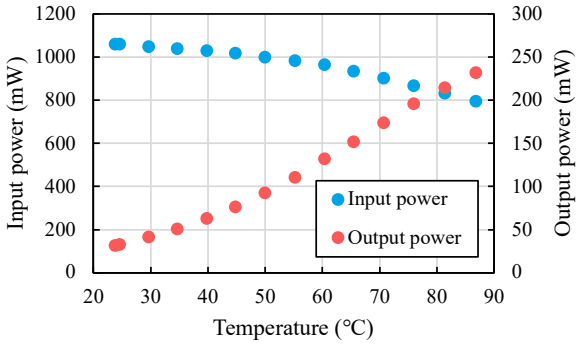

Fig. 11. Input and output power with respect to temperature change.

increased so that the output power P_2 does not exceed the rated power of the thermistor. Fig. 9 shows the coils attached to the shaft of the rotor taken from the PMSM. The air gap between the coils is 5 mm.

B. Experimental result

Fig. 10 shows the input/output voltage and current waveforms of the WPT system with the coils mounted on the shaft. As in the experiment without a shaft, the resonant operation of the WPT circuit is maintained at different temperatures even if the shaft is inserted.

Fig. 11 shows the change in the input and output power with respect to temperature change when the shaft of the motor is

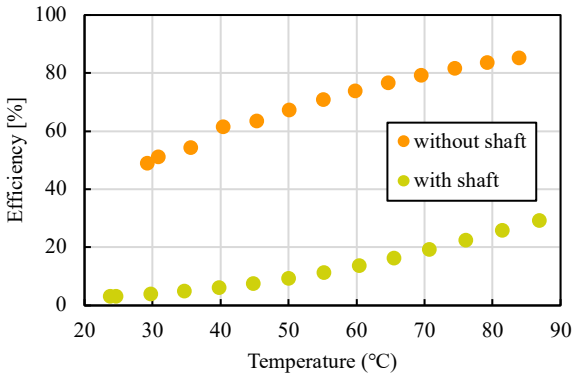

Fig. 12. AC-AC efficiency vs. temperature with and without shaft.

inserted into the coils. As in the experiment without a shaft, the input power decreases monotonically as the temperature of the thermistor rises. However, the output power increases as the temperature rises, even though the output power decreases in the experiment without the shaft.

Fig. 12 shows a comparison of AC-to-AC efficiency regarding thermistor temperature with and without a shaft. It is observed that mounting the coils around the shaft significantly reduced efficiency. This is estimated as the effect of iron loss caused by the magnetic flux emitted by the coil chaining to the steel shaft. In the proposed system, the characteristics of the input power with respect to the thermistor temperature are important, and efficiency is not important. Therefore, low efficiency is not a significant problem. However, if the iron loss is too significant, the power consumed by the thermistor will be relatively small. This may make it challenging to observe power changes with respect to temperature changes. It was demonstrated that the power and efficiency characteristics of the circuit were changed with or without the shaft.

VI. Conclusion

A temperature detection system using WPT has been proposed to detect the temperature of magnets in the rotor of a PMSM. The proposed system detects the PMSM magnet temperature as the input power of the WPT system. In this paper, a prototype WPT system was designed so that the output power of the WPT system does not exceed the power rating of the NTC thermistor connected as the load. Experimental results with the designed prototype show that the input power decreases monotonically with increasing temperature of the thermistor. This result shows that the temperature change of the thermistor is detected through the change in the input power. In addition, an experiment was conducted with the coil with the shaft of the rotor, assuming that the proposed system would be attached to a PMSM. The experimental results indicate that a large iron loss occurs on the shaft. In future work, a design of the proposed system will be presented while considering the effect of iron loss on the shaft.

References

[1] MEIT, MLIT, “Document 2 ‘Scope of regulation’,” 6th Joint Meeting of Automobile Judgment Standards Working Group of Energy Conservation Subcommittee of Energy Conservation and New Energy Subcommittee of Advisory Committee for Natural Resources and Energy and Automobile Fuel Efficiency Standards Subcommittee of Automobile Subcommittee of Land Transport Subcommittee of Council for Transport Policy, 2011.

[2] Y. Tasaka, “PMSM propulsion system for rolling stock,” Toshiba Review, vol. 68, no. 4, pp. 23-26, 2013

[3] K. Miyata, Y. Aoyama, T. Yokoyama, K. Ohashi, M. Kondo, and K. Matsuoka, “3-D magnetic field analysis of permanent magnet motor considering magnetizing, demagnetizing and eddy current loss,” IEEJ Trans. IA, vol. 123, no. 4, pp. 401-408, 2003

[4] M. Nakano, H. Kometani, M. Kawamura, and K. Miyata, “Estimation technology of thermal demagnetization in permanent magnet motors,” Mitsubishi Denki giho, vol. 79, no. 11, pp. 19-22, 2005

[5] MATSUI Corporation, “Telemeter of Manner Sensortelemetrie GmbH,” Technical sheet, no. TM-002-06, 2013

[6] A. Ito, K. Ohishi, Y. Yokokura, Y. Ide, D. Kuraishi, A. Takahashi, and M. Kitahara, “Simultaneous temperature estimation of winding and magnet of pmsm by high-frequency-injection into static coordinate,” IEEJ The papers of Joint Technical Meeting on “Semiconductor Power Converter” and “Motor Drive”, SPC-22-166/MD-22-101, pp. 127-132, 2022

[7] M. Kamiya, H. Awata, T. Miura, Y. Yagyu, T. Kosaka, and N. Matsui, “Permanent magnet temperature analysis considering pwm carrier harmonics for interior permanent magnet synchronous generator in hybrid vehicles,” IEEJ Trans. IA, vol. 127, no. 12, pp. 1238-1244, 2007

[8] Y. Imanishi and S. Nishiguchi, “Development of temperature estimation for motor magnet of electric vehicle,” SAEJ Trans., vol. 45, no. 5, pp.841-845, 2014

[9] Y. Hojo, “Temperature detection system,” Patant No. 7201462, January 2019

[10] Vishay Intertechnology Inc., “Selecting NTC Thermistors,” July 2015

[11] Vishay Intertechnology Inc., “NTCLG100E2,” June 2017